

# Low-Complexity Detection of OFDM in Doubly-Dispersive Channels

Philip Schniter and Siddharth D'Silva

Dept. of Electrical Engineering  
The Ohio State University  
Columbus, OH 43210  
schniter.1@osu.edu, dsilva.1@osu.edu

## Abstract

*When OFDM systems with large block length are used in fast-fading multipath channels, the channel may induce significant inter-carrier interference (ICI). As a result, the standard ML, MMSE and ZF detectors become prohibitively complex. In response, we propose a computationally-efficient decision-feedback detection strategy based on optimal windowing and linear MMSE estimation. Simulation results indicate good performance relative to the standard MMSE detector but with significant computational savings.*

## 1 Introduction

While the application of orthogonal frequency division multiplexing (OFDM) in slow-fading frequency-selective (FS) channels is well understood (e.g., [1, 2, 3, 4]), the application of OFDM in fast-fading FS channels results in new challenges (e.g., [5, 6, 7]), many of which have not been practically treated in the literature.

Current trends in broadband communication systems lead us to believe that channel time-variation will soon play an important role in OFDM systems. First, as communication systems are implemented in higher frequency bands (e.g.,  $\gg 1$  GHz) and thus using smaller wavelengths, the sensitivity of channel parameters to physical movement grows proportionally. In other words, effective rates of channel variation for a fixed mobile speed increase. Second, increasing either the efficiency or the bandwidth of an OFDM system will increase the sensitivity to channel variation. This latter claim can be understood from the desire to have a large OFDM block length which allows, in turn, significant channel variation within a block. Large block length is motivated by the desire to i) reduce capacity loss due to insertion of redundant guard intervals, and ii) maintain narrow subcarrier spacing (to ensure flat subcarrier fading) as system bandwidth increases. Channels that exhibit fast time-selective fading lead to a loss

of OFDM subcarrier orthogonality resulting in ICI. Thus, the primary motivation for OFDM in FS channels—the absence of ICI—does not carry over to time- and frequency-selective, i.e., doubly-selective channels.

## 2 OFDM System Model

Before analyzing the effects of channel time-variation on OFDM systems, we first review the system model. The OFDM transmitter parses the incoming (coded) bit-stream into blocks of  $N$  “frequency-domain” QAM symbols, each of which gets transformed into a block of “time-domain” transmitted samples using an  $N$ -point inverse FFT. To prevent inter-block interference at the receiver and to ensure a circular (rather than linear) convolution with the channel response, the time-domain blocks are cyclically prepended prior to transmission with an extension length at least as long as the channel impulse response. The time-domain blocks are then serially transmitted through a multipath fading channel, modeled as a discrete linear time-varying (LTV) system characterized by  $h_{t,l}(n, m)$ , the response at time  $n$  to an impulse applied at time  $n - m$ , before corruption by zero-mean circular white Gaussian noise  $\tilde{w}(n)$ . The OFDM receiver observes the output of the noisy linear channel and discards the samples corresponding to the prefix, after which the time-domain observation sequence for a single OFDM block can be written in vector form as

$$\mathbf{x}_t = \mathcal{H}_{t,l} \mathbf{F}^H \mathbf{s} + \tilde{\mathbf{w}} \quad (1)$$

In (1),  $\mathbf{s}$  denotes a vector of frequency-domain QAM symbols,  $\mathbf{F}^H$  a unitary matrix representing the inverse  $N$ -FFT operation,  $\mathcal{H}_{t,l}$  a matrix representing the time-domain effect of the channel and  $\tilde{\mathbf{w}}$  a vector of time-domain noise samples. When the channel is linear time-invariant (LTI),  $\mathcal{H}_{t,l}$  is circulant.

Performing a FFT (denoted by  $\mathbf{F}$ ) at the receiver, we obtain the frequency-domain observation vector

$$\mathbf{x}_f = \mathbf{F} \mathbf{x}_t = \mathbf{F} \mathcal{H}_{t,l} \mathbf{F}^H \mathbf{s} + \mathbf{F} \tilde{\mathbf{w}} = \mathcal{H}_{d,f} \mathbf{s} + \mathbf{w} \quad (2)$$



and “noise + interference” energies are

$$\begin{aligned}\mathcal{E}_s &= \frac{1}{N} \|\mathcal{M}(\mathcal{C}(\mathbf{B})\mathcal{H}_{d,f})\|_F^2 \\ \mathcal{E}_{ni} &= \frac{1}{N} \|\overline{\mathcal{M}}(\mathcal{C}(\mathbf{B})\mathcal{H}_{d,f})\|_F^2 + \frac{\sigma_w^2}{N} \|\mathcal{C}(\mathbf{B})\|_F^2\end{aligned}$$

where  $\|\cdot\|_F$  denotes the Frobenius norm.

## 4.2 Max-SINR Window Design

Ideally, the ICI-shortening window should be optimized to maximize symbol detection performance. If we assume an OFDM system employing powerful error-control coding, then the performance will be proportional to the average signal to interference-plus-noise ratio (SINR) across carriers [11], which motivates a window design maximizing average carrier SINR.

From (4) and Fig. 1, we are motivated to choose an “adjacent-carrier” desired ICI region, i.e.,  $\mathcal{C}(\mathbf{B})\mathcal{H}_{d,f}$  with a banded structure (including the top-right and bottom-left corners). Equivalently, the mask operator  $\mathcal{M}(\cdot)$  nulls the  $\nu^{th}$  diagonal for each  $\nu$  in the range  $D+1 \leq \langle \nu \rangle_N \leq N-D-1$ , where  $\nu=0$  corresponds to the main diagonal. The parameter  $D$  controls the target level of ICI shortening: smaller  $D$  corresponds to a shorter ICI span and thus reduced detection complexity. While technically we require  $0 \leq D \leq \frac{N}{2}-1$ , we have observed that, for good window performance,  $D$  must be chosen in accordance with the Doppler spread.

Our definition of  $\mathcal{M}(\cdot)$  allows the simplification

$$\|\mathcal{M}(\mathcal{C}(\mathbf{B})\mathcal{H}_{d,f})\|_F^2 = \|\mathcal{P}\mathcal{C}(\mathbf{B})\mathbf{H}_{d,f}\|_F^2$$

where  $\mathbf{H}_{d,f}$  is a re-arrangement of  $\mathcal{H}_{d,f}$  defined by

$$[\mathbf{H}_{d,f}]_{\nu,k} = h_{d,f}(\nu, k).$$

and

$$\mathcal{P} = \begin{bmatrix} \mathbf{I}_{D+1} & \mathbf{0} & \mathbf{0} \\ \mathbf{0} & \mathbf{0} & \mathbf{0} \\ \mathbf{0} & \mathbf{0} & \mathbf{I}_D \end{bmatrix}$$

Similarly, we can use  $\mathcal{P}^\perp = \mathbf{I}_N - \mathcal{P}$  to say

$$\|\overline{\mathcal{M}}(\mathcal{C}(\mathbf{B})\mathcal{H}_{d,f})\|_F^2 = \|\mathcal{P}^\perp \mathcal{C}(\mathbf{B})\mathbf{H}_{d,f}\|_F^2.$$

Maximizing SINR  $\mathcal{E}_s/\mathcal{E}_{ni}$  is accomplished by

$$\begin{aligned}\mathbf{b}_* &= \arg \max_{\mathbf{b}} \frac{\|\mathcal{P}\mathcal{C}(\mathbf{B})\mathbf{H}_{d,f}\|_F^2}{\|\mathcal{P}^\perp \mathcal{C}(\mathbf{B})\mathbf{H}_{d,f}\|_F^2 + \sigma_w^2 \|\mathcal{C}(\mathbf{B})\|_F^2} \\ &= \arg \max_{\mathbf{b}} \frac{\|\mathcal{P}\mathcal{F}\mathcal{D}(\mathbf{b})\tilde{\mathbf{H}}_{t,l}\|_F^2}{\mathbf{b}^H \text{diag}(\sigma_w^2 \mathbf{I} + \mathbf{H}_{t,l} \mathbf{H}_{t,l}^H) \mathbf{b} - \|\mathcal{P}\mathcal{F}\mathcal{D}(\mathbf{b})\tilde{\mathbf{H}}_{t,l}\|_F^2}\end{aligned}$$

where  $[\mathbf{H}_{t,l}]_{n,m} = h_{t,l}(n, m)$ . This can be solved in closed form through

$$\begin{aligned}\tilde{\mathbf{b}} &= \text{diag}(\sigma_w^2 \mathbf{I} + \mathbf{H}_{t,l} \mathbf{H}_{t,l}^H)^{\frac{1}{2}} \mathbf{b} \\ \tilde{\mathbf{b}}_* &= \arg \max_{\tilde{\mathbf{b}}} \frac{\|\mathcal{P}\mathcal{F}\mathcal{D}(\tilde{\mathbf{b}})\tilde{\mathbf{H}}_{t,l}\|_F^2}{\|\tilde{\mathbf{b}}\|^2 - \|\mathcal{P}\mathcal{F}\mathcal{D}(\tilde{\mathbf{b}})\tilde{\mathbf{H}}_{t,l}\|_F^2}\end{aligned}$$

using

$$\tilde{\mathbf{H}}_{t,l} = \text{diag}(\sigma_w^2 \mathbf{I} + \mathbf{H}_{t,l} \mathbf{H}_{t,l}^H)^{-\frac{1}{2}} \mathbf{H}_{t,l} \quad (7)$$

Since SINR is invariant to the scaling of  $\tilde{\mathbf{b}}$ , we assume w.l.o.g. that  $\|\tilde{\mathbf{b}}\| = 1$ , in which case

$$\tilde{\mathbf{b}}_* = \arg \max_{\|\tilde{\mathbf{b}}\|=1} \|\mathcal{P}\mathcal{F}\mathcal{D}(\tilde{\mathbf{b}})\tilde{\mathbf{H}}_{t,l}\|_F^2$$

It helps to rewrite the above norm as

$$\begin{aligned}\|\mathcal{P}\mathcal{F}\mathcal{D}(\tilde{\mathbf{b}})\tilde{\mathbf{H}}_{t,l}\|_F^2 &= \sum_{m=0}^{N_h-1} \sum_{|k| \leq D} \left| \frac{1}{\sqrt{N}} \sum_{n=0}^{N-1} \tilde{b}_n e^{-j \frac{2\pi k}{N} n} \tilde{h}_{t,l}(n, m) \right|^2 \\ &= \frac{1}{N} \sum_{n,l} \tilde{b}_n \tilde{b}_l^* \sum_{|k| \leq D} e^{-j \frac{2\pi(n-l)}{N} k} \\ &\quad \cdot \sum_{m=0}^{N_h-1} \tilde{h}_{t,l}(n, m) \tilde{h}_{t,l}^*(l, m) \\ &= \tilde{\mathbf{b}}^H \mathbf{A} \tilde{\mathbf{b}}\end{aligned}$$

where, using  $\odot$  to denote element-wise multiplication,

$$\begin{aligned}\mathbf{A} &= \frac{1}{N} \sum_{|k| \leq D} e^{-j \frac{2\pi(n-l)}{N} k} \cdot \sum_{m=0}^{N_h-1} \tilde{h}_{t,l}(n, m) \tilde{h}_{t,l}^*(l, m) \quad (8) \\ &= \mathbf{A}_1 \odot \mathbf{A}_2 \quad \text{for} \quad \begin{cases} [\mathbf{A}_1]_{l,n} = \frac{1}{N} \frac{\sin(\frac{\pi}{N}(2D+1)(n-l))}{\sin(\frac{\pi}{N}(n-l))} \\ \mathbf{A}_2 = (\tilde{\mathbf{H}}_{t,l} \tilde{\mathbf{H}}_{t,l}^H)^* \end{cases} \quad (9)\end{aligned}$$

Thus  $\tilde{\mathbf{b}}_*$  is the principle eigenvector of  $\mathbf{A}$  and

$$\mathbf{b}_* = \text{diag}(\sigma_w^2 \mathbf{I} + \mathbf{H}_{t,l} \mathbf{H}_{t,l}^H)^{-\frac{1}{2}} \tilde{\mathbf{b}}_* \quad (10)$$

Fig. 2 illustrates the effect of  $N$ -point max-SINR windowing on a representative realization of  $\mathcal{H}_{d,f}$ .

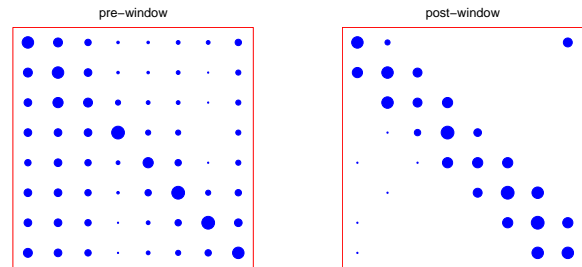


Figure 2: Typical effect of  $N$ -point max-SINR windowing on  $\mathcal{H}_{d,f}$ . (Dot size proportional to coefficient log-magnitude.)

## 4.3 Max-SINR Window Approximation

Calculation of the optimal window (10) requires knowledge of current channel coefficients. We now seek a channel-independent approximation to (10). From (7) and (9), we see that  $\mathbf{A}_2$  can be expanded into

$$\begin{aligned}\mathbf{A}_2 &= \text{diag}(\sigma_w^2 \mathbf{I} + \mathbf{H}_{t,l} \mathbf{H}_{t,l}^H)^{-\frac{1}{2}} (\mathbf{H}_{t,l} \mathbf{H}_{t,l}^H)^* \\ &\quad \cdot \text{diag}(\sigma_w^2 \mathbf{I} + \mathbf{H}_{t,l} \mathbf{H}_{t,l}^H)^{-\frac{1}{2}}\end{aligned}$$

With large delay-spread (i.e., large  $N_h$ ), we can approximate the summation in  $\mathbf{H}_{t,l}\mathbf{H}_{t,l}^H$  using an expectation:

$$\begin{aligned} [\mathbf{H}_{t,l}\mathbf{H}_{t,l}^H]_{n,l} &\approx \mathbb{E} \left\{ \sum_{m=0}^{N_h-1} h_{t,l}(n,m)h_{t,l}^*(l,m) \right\} \\ &= \sum_{m=0}^{N_h-1} \sigma_m^2 J_0(2\pi f_d(n-l)) \end{aligned}$$

since our WSSUS/Rayleigh assumption implies

$$\mathbb{E}\{h_{t,l}(n,m)h_{t,l}^*(l,p)\} = \begin{cases} 0 & m \neq p \\ \sigma_m^2 J_0(2\pi f_d(n-l)) & m = p \end{cases}$$

The max-SINR window quantities then become

$$\begin{aligned} \mathbf{b}_* &\approx \left( \sigma_w^2 + \sum_{m=0}^{N_h} \sigma_m^2 \right)^{-\frac{1}{2}} \tilde{\mathbf{b}}_* \\ [\mathbf{A}_2]_{l,n} &\approx \left( \frac{\sum_{m=0}^{N_h} \sigma_m^2}{\sigma_w^2 + \sum_{m=0}^{N_h} \sigma_m^2} \right) J_0(2\pi f_d(n-l)) \end{aligned}$$

As desired, an approximate max-SINR window can be constructed using channel and noise *statistics* rather than channel *realizations*. Furthermore,  $\sigma_w^2$  and  $\sigma_m^2$  only affect window scaling and not the resulting SINR. Thus the window coefficients need only be a function of  $f_d$ ,  $D$  and  $N$ .

In Fig. 3 we plot SINR ( $\mathcal{E}_s/\mathcal{E}_{ni}$ ) versus symbol-to-noise power ratio for an OFDM system with  $N = 128$ ,  $N_h = 32$ , and various values of  $f_d$ . The benefits of windowing are clear. Observe that the max-SINR window (from Sec. 4.2) and its realization-independent approximation (from Sec. 4.3) have nearly identical performance.

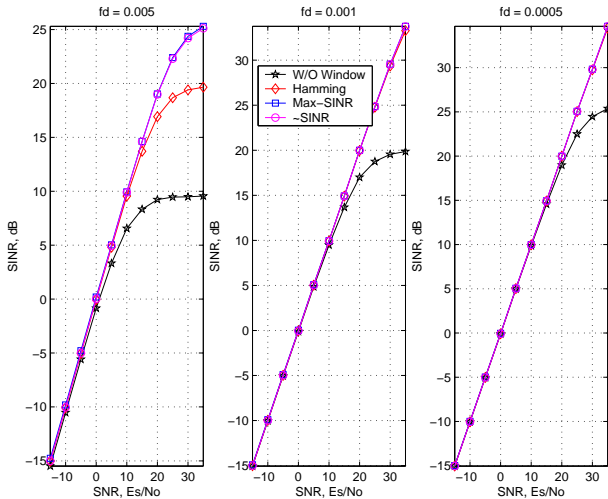


Figure 3: Post-windowing SINR ( $\mathcal{E}_s/\mathcal{E}_{ni}$ ) vs. SNR ( $\mathcal{E}_s/N_o$ ).

## 5 MMSE-based Decision-Feedback

Say that a max-SINR window has been designed with particular ICI-range  $D$  (as defined in Sec. 4). The windowed reception  $\bar{\mathbf{x}}_f$  can be written in terms of signal and interference components as

$$\bar{\mathbf{x}}_f = \bar{\mathcal{H}}_{d,f} \mathbf{s} + \bar{\mathbf{w}}$$

where, as illustrated in Fig. 4(a),

$$\bar{\mathcal{H}}_{d,f} = \frac{1}{\sqrt{N}} \mathcal{M}(\mathcal{C}(\mathbf{B})\mathcal{H}_{d,f})$$

$$\bar{\mathbf{w}} = \frac{1}{\sqrt{N}} \left( \bar{\mathcal{M}}(\mathcal{C}(\mathbf{B})\mathcal{H}_{d,f})\mathbf{s} + \mathcal{C}(\mathbf{B})\mathbf{w} \right)$$

If the first  $D$  and last  $D$  elements of  $\mathbf{s}$  are known or suppressed pilots, the relationship between the unknown symbols  $\mathbf{s}_u$  and the windowed frequency domain observation *after pilot removal* can be written  $\bar{\mathbf{x}} = \tilde{\mathcal{H}}_{d,f} \mathbf{s}_u + \bar{\mathbf{w}}$ , where  $\tilde{\mathcal{H}}_{d,f}$  has the banded structure shown in Fig. 4(b).

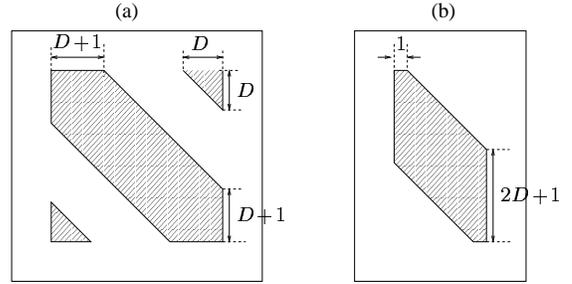


Figure 4: General structure of (a)  $\bar{\mathcal{H}}_{d,f}$  and (b)  $\tilde{\mathcal{H}}_{d,f}$ .

Noting that all information about the last element in  $\mathbf{s}_u$  is contained in the  $2D+1$  last elements of  $\bar{\mathbf{x}}$ , we can set up the relation  $\bar{\mathbf{x}}^{(1)} = \tilde{\mathcal{H}}_{d,f}^{(1)} \mathbf{s}_u^{(1)} + \bar{\mathbf{w}}^{(1)}$  where  $\bar{\mathbf{x}}^{(1)}$ ,  $\mathbf{s}_u^{(1)}$ ,  $\bar{\mathbf{w}}^{(1)}$  are the last  $2D+1$  entries in  $\bar{\mathbf{x}}$ ,  $\mathbf{s}_u$ ,  $\bar{\mathbf{w}}$  respectively and  $\tilde{\mathcal{H}}_{d,f}^{(1)}$  is the  $(2D+1) \times (2D+1)$  upper triangular matrix formed by the last  $2D+1$  rows and columns of  $\tilde{\mathcal{H}}_{d,f}$ . Fig. 5(a) shows the basic structure of  $\tilde{\mathcal{H}}_{d,f}$  for  $D = 1$  with the dashed region identifying  $\tilde{\mathcal{H}}_{d,f}^{(1)}$ . With channel knowledge, we can perform linear-MMSE estimation of the last element in  $\mathbf{s}_u^{(1)}$  using an  $\mathcal{O}(D^3)$  matrix inverse:

$$\begin{aligned} [\hat{\mathbf{s}}_u^{(1)}]_{2D+1} &= \\ &\mathbf{e}_{2D+1}^H \tilde{\mathcal{H}}_{d,f}^{(1)H} \left( \tilde{\mathcal{H}}_{d,f}^{(1)} \tilde{\mathcal{H}}_{d,f}^{(1)H} + \sigma_w^2 \mathbf{C}^{(1)} \mathbf{C}^{(1)H} \right)^{-1} \bar{\mathbf{x}}^{(1)} \end{aligned}$$

Above we used the fact that  $\bar{\mathbf{w}}^{(1)} \sim \mathcal{N}(\mathbf{0}, \sigma_w^2 \mathbf{C}^{(1)} \mathbf{C}^{(1)H})$ , where  $\mathbf{C}^{(1)}$  is a matrix containing the  $2D+1$  last rows of  $\mathcal{C}(\mathbf{B})$  and  $\mathbf{e}_{2D+1}$  is a length  $2D+1$  unit vector given by  $\mathbf{e}_{2D+1} = [0, \dots, 0, 1]^H$ . Having estimated the last element in  $\mathbf{s}_u$ , a tentative decision can be fed back to cancel this symbol's contribution to  $\bar{\mathbf{x}}$  using the last column of  $\tilde{\mathcal{H}}_{d,f}$  as shown in Fig. 5(b). Now the second-to-last element of  $\mathbf{s}_u$  can be MMSE estimated using the same procedure. This process can be repeated until only the first

$2D+1$  elements of  $\mathbf{s}_u$  remain as shown in Fig. 5(d). These remaining symbols can be jointly detected using a linear MMSE scheme.

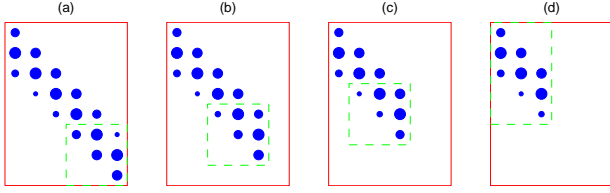


Figure 5: MMSE-based decision-feedback detection.

## 6 Simulations and Conclusions

In Fig. 6 we plot the performance of the  $\mathcal{O}(N^3)$  linear MMSE detector (3) and the  $\mathcal{O}(D^3N)$  MMSE-based decision-feedback detector described in Sec. 5. The OFDM system employed QPSK and block length  $N = 128$ . The channel was WSSUS Rayleigh with delay spread  $N_h = 32$  and normalized Doppler  $f_d = 0.001$  in (a) and  $f_d = 0.01$  in (b). Bit error probability was calculated as

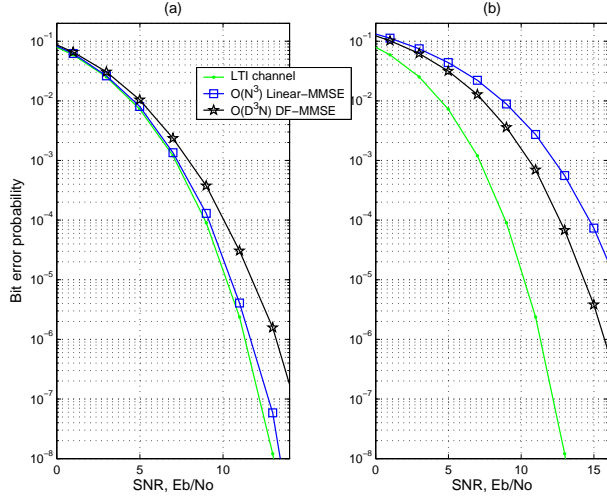


Figure 6: Comparison of different detectors.

follows. First, Jakes' method was used to generate fading channel realizations over a span of many blocks. For *each* block, the SINRs of symbol estimates were computed at each subcarrier, averaged over the  $N$  subcarriers, and then converted to BER assuming Gaussian interference. Finally, these BERs were averaged over a large number of blocks. As discussed previously, carrier-averaging was employed to mimic the use of heavy coding. The "LTI channel" traces in Fig. 6 were included as a reference; they reflect the case where the channel remains fixed throughout each block but changes between blocks.

Fig. 6 demonstrates that the decision-feedback scheme offers good performance relative to the linear MMSE de-

tor. When  $f_d = 0.001$ , the  $\mathcal{O}(N^3)$  linear detector outperforms the  $\mathcal{O}(D^3N)$  decision-feedback detector at the cost of a much greater complexity. When  $f_d = 0.01$ , however, the decision-feedback detector outperforms the linear detector even though the former is much simpler to implement! This can be understood by the fact that the decision-feedback detector employs non-linear processing to leverage receiver knowledge of the finite-alphabet constellation.

Future research directions will investigate improved linear pre-processing, more sophisticated detection algorithms (e.g., "turbo" methods), the effect of practical coding, and low-complexity channel identification.

## References

- [1] S. B. Weinstein and P. M. Ebert, "Data transmission by frequency division multiplexing using the discrete Fourier transform," *IEEE Trans. on Communications*, vol. 19, pp. 628–634, Oct. 1971.
- [2] L. J. Cimini, Jr., "Analysis and simulation of a digital mobile radio channel using orthogonal frequency division multiplexing," *IEEE Trans. on Communications*, vol. 33, pp. 665–765, July 1985.
- [3] J. A. C. Bingham, "Multicarrier modulation for data transmission: An idea whose time has come," *IEEE Communications Magazine*, vol. 28, pp. 5–14, May 1990.
- [4] S. B. Bulumulla, S. A. Kassam, and S. S. Venkatesh, "A systematic approach to detecting OFDM signals in a fading channel," *IEEE Trans. on Communications*, vol. 48, pp. 725–728, May 2000.
- [5] B. Stantchev and G. Fettweis, "Time-variant distortions in OFDM," *IEEE Communications Letters*, vol. 4, pp. 312–314, Oct. 2000.
- [6] P. Robertson and S. Kaiser, "The effects of Doppler spreads on OFDM(A) mobile radio systems," in *Proc. IEEE Vehicular Technology Conference*, vol. 1, pp. 329–333, 1999.
- [7] Y. H. Kim, I. Song, H. G. Kim, T. Chang, and H. M. Kim, "Performance analysis of a coded OFDM system in time-variant multipath Rayleigh fading channels," *IEEE Trans. on Vehicular Technology*, vol. 48, no. 5, pp. 1610–1615, 1999.
- [8] W. C. Jakes, *Microwave Mobile Communications*. Wiley, 1974.
- [9] S. D'Silva, "On OFDM in doubly-dispersive channels," Master's thesis, The Ohio State University, Dec. 2002.
- [10] D. D. Falconer and F. R. Magee, "Adaptive channel memory truncation for maximum likelihood sequence estimation," *Bell System Technical Journal*, vol. 52, pp. 1541–1562, Nov. 1973.
- [11] H. Sari, G. Karam, and I. Jeanclaude, "Transmission techniques for digital terrestrial TV broadcasting," *IEEE Communications Magazine*, pp. 100–109, Feb. 1995.